Pulsatile Flow Characterization in a Vessel Phantom With Elastic Wall Using Ultrasonic Particle Image Velocimetry Technique: The Impact of Vessel Stiffness on Flow Dynamics

Ming Qian*, *Member, IEEE*, Lili Niu, Kelvin Kian Loong Wong, Derek Abbott, *Fellow, IEEE*, Qifa Zhou, *Senior Member, IEEE*, and Hairong Zheng*, *Senior Member, IEEE*

***Abstract*—This study aims to experimentally investigate the impact of vessel stiffness on the flow dynamics of pulsatile vascular flow. Vessel phantoms with elastic walls were fabricated using polyvinyl alcohol cryogel to result in stiffness ranging from 60.9 to 310.3 kPa and tested with pulsatile flows using a flow circulation set-up. Two-dimensional instantaneous and time-dependent flow velocity and shear rate vector fields were measured using ultrasonic particle image velocimetry (EchoPIV). The waveforms of peak velocities measured by EchoPIV were compared with the ultrasonic pulse Doppler spectrum, and the measuring accuracy was validated. The cyclic vessel wall motion and flow pressure were obtained as well. The results showed that vessel stiffening influenced the waveforms resulting from vessel wall distension and flow pressure, and the fields of flow velocity and shear rate. The stiffer vessel had smaller inner diameter variation, larger pulse pressure and median pressure. The velocity and shear rate maximized at peak systole for all vessels. The results showed a decrease in wall shear stress for a stiffer vessel, which can initiate the atherosclerotic process. Our study elucidates the impact of vessel stiffness on several flow dynamic parameters, and also demonstrates the EchoPIV technique to be a useful and powerful tool in cardiovascular research.**

***Index Terms*—Flow velocity, polyvinyl alcohol (PVA) cryogel, shear rate, ultrasonic particle image velocimetry, vessel stiffness.**

Manuscript received January 9, 2014; revised April 15, 2014; accepted April 21, 2014. Date of publication April 30, 2014; date of current version August 18, 2014. This work was supported in part by the National Science Foundation Grants (11272329), in part by the National Key Technology R&D Program of China (2012BAI13B01), in part by the Guangdong Research Grant (2011A030300016), and in part by the Shenzhen International Collaboration Grant (GJHZ20120617111428312). M. Qian and L. Niu are co-first authors. *Asterisk indicates corresponding author*.

*M. Qian is with the Shenzhen Institutes of Advanced Technology, Chinese Academy of Sciences, Shenzhen 518055, China (e-mail: ming.qian@siat.ac.cn).

L. Niu is with the Shenzhen Institutes of Advanced Technology, Chinese Academy of Sciences, Shenzhen 518055, China (e-mail: ll.niu@siat.ac.cn).

K. K. L. Wong and D. Abbott are with the Centre for Biomedical Engineering, and School of Electrical and Electronic Engineering, University of Adelaide, Adelaide SA5005, Australia (e-mail: k.wong@rmit.edu.au; derek.abbott@adelaide.edu.au).

Q. Zhou is with the NIH Ultrasonic Transducer Resource Center and Department of Biomedical Engineering, University of Southern California, CA 90089 USA (e-mail: qifazhou@usc.edu).

*H. Zheng is with the Shenzhen Institutes of Advanced Technology, Chinese Academy of Sciences, Shenzhen 518055, China (e-mail: hr.zheng@siat.ac.cn).

Color versions of one or more of the figures in this paper are available online at http://ieeexplore.ieee.org.

Digital Object Identifier 10.1109/TBME.2014.2320443

I. Introduction

It has been known for over two centuries that the integrated effect of hemodynamics and arterial wall mechanics plays a fundamental role in cardiovascular health [1], [2]. Measuring the details of flow in arterial models or artificial organs is essential to investigate various flow-induced changes, and to evaluate patient-specific parameters such as geometry, non-Newtonian flow characteristics, wall elasticity, and steady and pulsatile flow [3]–[7]. Techniques that can assess diseased arteries via flow information and vascular mechanics can provide insight into the diagnostic or therapeutic management of cardiovascular diseases (CVD). Till now, many studies have been performed. However, the experiments on the impact of arterial stiffness on blood flow dynamic parameters are seldom reported.

In clinical practice, the changes in blood flow dynamics have been used to diagnose the location and extent of disease. Ultrasound-based techniques have gained broad applications for the purpose of blood flow imaging due to the advantages of real time, cheap, easy to use, safe and nonionizing. The pulsed wave Doppler technique is routinely used to obtain 1-D time-dependent blood flow velocity information [8], [9], but the typical limitation of this technique is angle dependence. In order to overcome this limitation, and to obtain more accurate 2-D blood flow velocity patterns, many novel ultrasound-based techniques have been developed in the past two decades, including ultrasonic speckle velocimetry [10], vector flow imaging using plane wave excitation [11], ultrasonic perpendicular velocimetry [12], and ultrasonic particle image velocimetry (EchoPIV) [13], [14]. These techniques not only provide a better way to understand the flow velocity distribution but also can result in more accurate shear stress calculations. Based on this, the impact of hemodynamic shear stress on the arterial wall has been studied [15], [16]. The innermost intima vessel layer is exposed to both wall stress caused by pulsating blood pressure and wall shear stress (WSS) caused by pulsatile blood flow, and influences the many functions of endothelium that control the process of production and degradation [17].

More recently, researchers have been paying increasing attention to arterial stiffness, considering it to be both a diagnosis target and an important issue in the development of CVD. Changes in arterial stiffness may occur early in the atherosclerotic process, even before the anatomical changes of intima-media

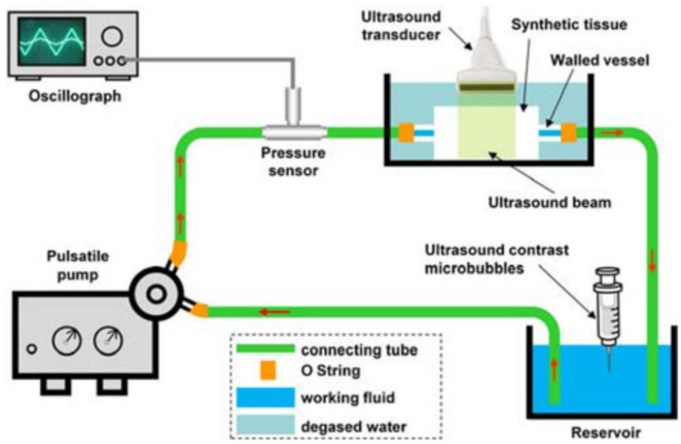

Fig. 1. Diagram of the experimental setup: the pump pushed the working fluid to circulate and flow through the vessel phantom with elastic walls; pulsatile flow was generated in the vessel; the flow pressure was recorded using the pressure sensor; the B-mode image sequences were acquired using the ultrasonix RP ultrasound system for postprocessing.

thickening become perceptible [18], [19], and arterial stiffening plays an important role in the process of CVD. A number of studies examined the ability of arterial stiffness to predict the risk of future fatal and nonfatal cardiovascular events and total mortality [20]–[22]. Correspondingly, several ultrasound-based techniques have been developed for arterial stiffness measurements, including pulse wave velocity (PWV) measurements [23], [24], regional PWV [25], [26], tissue Doppler [27], [28], phase-tracking [29], and an ultrasound image-based texture matching method [30]. Lately, Niu *et al*. have combined EchoPIV and image-based texture matching method to simultaneously measure arterial strain and flow pattern [31].

Till now, there have been limited experimental studies on how arterial stiffness can influence the blood flow dynamics and how arterial mechanics and blood flow interact, which provides the motivation of this study. In this paper, vessel phantoms with elastic walls were made using polyvinyl alcohol (PVA) cryogel in order to simulate human common carotid arteries of different stiffness. Then, the pulsatile flows within the vessels having variable stiffness were characterized using EchoPIV. The accuracy of EchoPIV measurements was demonstrated by comparing the waveforms of peak velocities with the ultrasonic Doppler spectrum. Importantly, 2-D detailed maps of blood flow and shear rate patterns, as well as waveforms of the vessel wall distension, flow pressure, and time-dependent flow velocity and shear rate were obtained, analyzed, and discussed.

II. Materials and Methods

A. Pulsatile Flow Circulation and Ultrasound Imaging System

A pulsatile flow was generated within an elastic vessel phantom using a flow circulatory test rig as shown in Fig. 1. An ultrasound system (Sonix RP, Ultrasonix, Canada) equipped with a linear transducer (L14-5W/60, transmit frequency 10 MHz) was used for data acquisition. The vessel was coated by synthetic tissue to simulate human common carotid artery surrounded by human tissue. The elastic vessel phantom had initial inner diameter of 6 mm, and underwent distension and contraction when pumped. The whole phantom was immersed in degassed water for the convenience of ultrasound beam transmission. An aqueous solution of ultrasound contrast microbubbles was used as the working fluid. The bubbles were generated using the mechanical agitation method and suspended in deionized water [32]. Each bubble consisted of octafluoropropane gas encapsulated by a phospholipid shell. Bubble concentration and size distribution were characterized using an AccuSizer 780A particle sizing system (Santa Barbara, CA, USA). Each milliliter of solution contained $1 \sim 2{\times}10^9$ bubbles. A major peak was observed at the size of 0.67 μm, with mean and median size of 1.90 and 0.93 μm, respectively. The working fluid (microbubbles aqueous solution) had a bubble concentration of 1×10^3 bubbles/ml. This concentration was chosen for the optimum quality of ultrasonic images, so as to maximize the accuracy of EchoPIV measurements [33].

The pulsatile pump (Model 55-3305, Harvard, USA), the vessel phantom, the pressure sensor (HDP708, Hedi Sensing Instrument, Guangdong, China), and the reservoir filled with the working fluid were connected using plastic tubes. The pump simulated the ventricular action of the heart and pushed the fluid to circulate. The stroke volume, stroke rate of the pump were maintained at 15 ml per stroke, 60 strokes per min in all experiments, so as to simulate the heart beat at 60 beats/min. The pressure sensor was connected to an oscillograph (DPO3032, Tektronix) for recording the flow pressure waveform, which was composed of systolic phase and diastolic phase. The peak systole was defined as the time point when the systolic pressure reaches maximum.

B. Phantom Fabrication and Characterization

The vessel phantoms with elastic walls coated with synthetic tissue were made from PVA cryogel (PVA-C). The PVA aqueous solution was filled into a steel mold, and then frozen and subsequently thawed to form a cryogel with rubber-like properties [34]. The composition (by weight) of the solution was 10% PVA powder, 87% deionized water, and 3% scattering particles (Sigma-Aldrich, USA). The mold consisted of a sleeve (14 mm inner diameter), two diaphragms (10 mm inner diameter and 14 mm outer diameter), a cylindrical rod (6 mm outer diameter), and two caps [see Fig. 2(a)]. All components except the upper cap were assembled, the solution was injected into the gap between the rod and the diaphragms, and the upper cap was then screwed [see Fig. 2(b)]. The whole mold underwent a number of (1 to 8) freeze–thaw (f–t) cycles to result in different stiffness. Each f–t cycle comprised of 12 h of freezing at -20 °C and 12 h of thawing at 20 °C. The obtained vessel phantoms with elastic walls had a regular concentric lumen and different stiffness. The vessel had 6 mm inner diameter, 10 mm outer diameter, and 16 cm length. The vessel with the inserted steel rod was assembled inside a glass tank, and the same PVA solution was gently poured into the tank to coat the vessel. The steel rod insured that the elastic tube did not deform. The whole tank was then subjected to one more f–t cycle. The vessel was covered with 2 cm of synthetic tissue [see Fig. 2(c)]. The synthetic

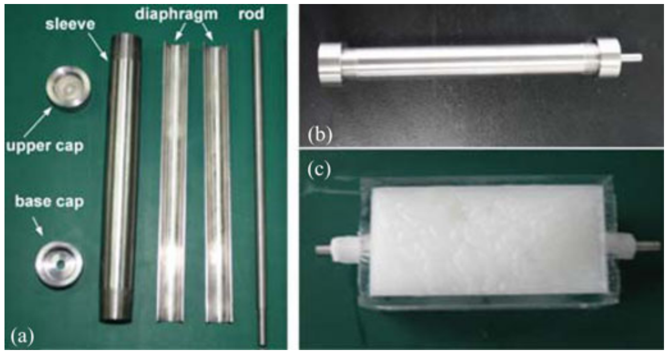

Fig. 2. Fabrication of the vessel phantoms with elastic walls coated with synthetic tissue: (a) the steel mold was composed of a sleeve with 14 mm inner diameter, two diaphragms with 10 mm inner diameter and 14 mm outer diameter, a cylindrical rod with 6 mm outer diameter, and two caps; (b) all the components except the upper cap were assembled together, and the PVA solution was injected into the gap, and the upper cap was then screwed; and (c) the resulted vessel phantoms with elastic walls surrounded by synthetic tissue.

tissue supported the vessel and guaranteed isotropic vessel wall motion. Three phantoms (3, 5, and 8 f–t cycles) were used in flow experiments.

The speed of sound within and the attenuation coefficient of the vessel samples were determined using the pulse–echo substitution method [35]. A 10 MHz single element transducer (Panametrics, Olympus, MA, USA) acted as both the transmitter and receiver. Young's modulus was measured using a CMT 6104 testing instrument (MTS System Corporation, China). Each sample was subjected to stress–strain cycles to a displacement of 15% of the gauge length. The Young's elastic moduli were calculated from the upward loading portion of the stress–strain curves. The modulus was evaluated as the mean gradient of the best-fit least-squares line to the data from 6%–15% [36].

C. Vessel Inner Diameter Measurements

Vessel diameter was automatically acquired from ultrasonic B-mode images. In sequential B-mode images, the boundaries between the flow and the walls were delineated using a region growing image segmentation method [37]. In this method, the intensity (or grayscale) difference in two consecutive frames of ultrasound contrast images was termed as window frame difference (WFD). The blood flow and microbubbles within move much faster than the arterial walls. Thus, there is much higher intensity variation in the lumen regions (microbubbles within) than in the arterial wall regions. Note that WFD information can, therefore, be used to segment these two regions. Our proposed segmentation method combines WFD and region growing algorithm to delineate the boundaries of the arterial walls from ultrasound contrast images and can automatically get the value of inner diameter.

D. Echo Particle Image Velocimetry Technique

The EchoPIV technique consists of identifying and tracking a tracer (ultrasound contrast microbubbles) within a flow field, and computing local velocity vectors using a cross-correlation algorithm. The B-mode images were acquired at a frame rate of 200 Hz using 128 ultrasound beams with focal depth of 2 cm and field of view of 3 cm (depth) by 3 cm (width). For each single data acquisition, more than 1200 frames were recorded, so as to cover at least five cardiac cycles. A new EchoPIV algorithm was used to process sequential image frames to get 2-D map of velocity vectors. This new algorithm made several improvements on the conventional PIV algorithm. A cross-correlation method was initially applied with a large interrogation window to estimate the displacement, and a multiple iterative algorithm was used to enhance the spatial resolution of the velocity measurements. Then, subpixel method, filter and interpolation method, and removal of spurious vectors were applied to improve the accuracy of velocity measurement. Please refer to [33] for more details about the algorithm. The 2-D flow velocity pattern allows detailed evaluation of the flow-mediated shear rate which can be calculated from the radial velocity gradient based on the following equation:

$$S = \frac{dv}{dr} \tag{1}$$

where v is the axial velocity, and r is the radial coordinate.

TABLE I
SPEED OF SOUND AND SOUND ATTENUATION FOR PHANTOMS OF DIFFERENT NUMBER OF F–T CYCLES

Number of f-t cycles	Speed of sound (m/s)	Sound attenuation (dB/cm)
1	1536.5	0.96
3	1543.2	1.31
5	1550.8	1.61
8	1552.1	1.70

III. RESULTS

A. Phantom Characterization

Five samples were prepared for each batch of phantoms that were subjected to the same number of f–t cycles, and the results of the five measurements were averaged. Table I lists the speed of sound and sound attenuation for phantoms of 1, 3, 5, and 8 f–t cycles. The speed of sound increased from 1536.5 to 1552.1 m/s. The synthetic tissue (1 f–t cycle) had a speed of sound of 1536.5 m/s, which was quite close to the routine value of 1540 m/s for human soft tissue. The speed of sound of the three phantoms (3, 5, and 8 f–t cycles) was close to the reported values for normal arteries [38]. The sound attenuation values at 10 MHz ranged from 0.96 to1.70 dB/cm.

The strain–stress curve is plotted for each vessel sample in Fig. 3(a). An increase in the mean Young's moduli with the number of f–t cycles was observed in Fig. 3(b). The 3, 5, and 8 f–t cycle phantom had modulus of 165.0, 250.5, and 310.3 kPa, respectively.

B. Flow Mediated Vessel Motions

The vessel dilated and contracted periodically (time period 1 s). The time-dependent curves of inner diameter (see Fig. 4) showed that it increased from a minimum at end diastole to a maximum at peak systole, and then declined to the minimum.

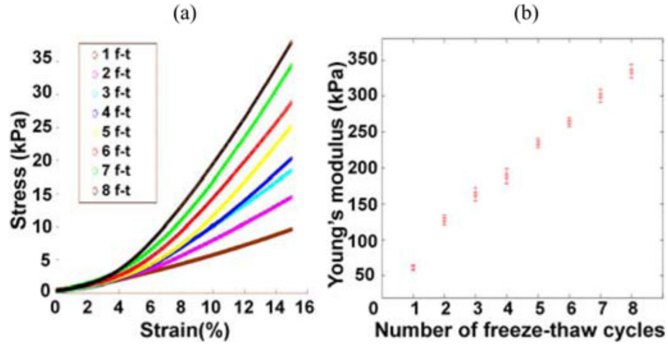

Fig. 3. Mechanical characteristics of vessel phantoms of different number of f–t cycles: (a) stress–strain curves; and (b) Young's modulus versus number of f–t cycles.

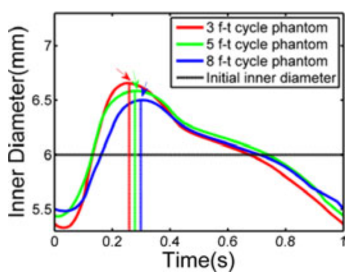

Fig. 4. Time-dependent curves of vessel inner diameter. The red, green, and blue solid curves correspond to the measured results of 3, 5, and 8 f–t cycle vessel, respectively. The black dotted line denotes the initial inner diameter for all the vessel phantoms. The red, green, and blue arrows point out the maximum diameters for the three vessel phantoms. The dotted vertical lines demonstrate the time points for the inner diameter achieving maximum.

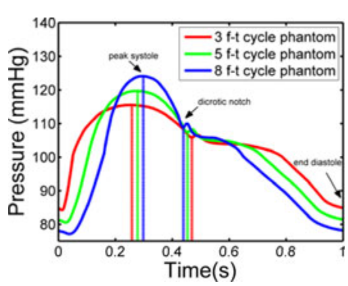

Fig. 5. Time-dependent pressure waveforms corresponding to different vessels: The red, green, and blue solid curves correspond to the measured results of 3, 5, and 8 f–t cycle vessel, respectively. The arrows point out peak systole, dicrotic notch, and end diastole. The dotted vertical lines demonstrate the time points for the pressure achieving systolic peak pressures and dicrotic notch.

For 3, 5, and 8 f–t cycle vessels, the maximum and minimum values were 6.69 and 5.30 mm, 6.61 and 5.40 mm, and 6.54 and 5.46 mm, respectively. The peak-to-peak diameter variation (1.39, 1.21, and 1.08 mm) became smaller as the vessel increased in stiffness. The time duration increased correspondingly (at 0.26, 0.28, and 0.30 s).

C. Flow Pressure Waveform

The recorded pressure was plotted against time in different colors (see Fig. 5). The pressure achieved maximum (113.9, 122.7, and 135.4 mmHg) at peak systole, and minimum (83.0, 79.3, and 74.7 mmHg) at end diastole. Pulse pressure (PP) was

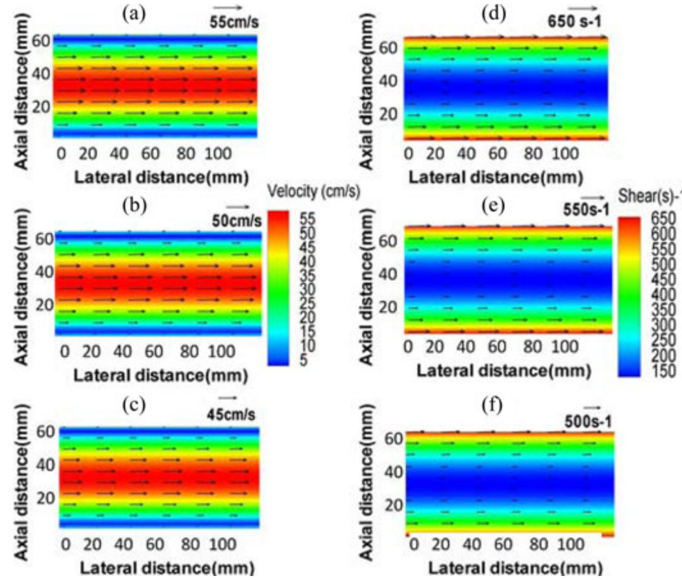

Fig. 6. Two-dimensional maps of flow velocity and shear at the peak systole: (a)–(c), velocity maps of 3, 5, and 8 f–t cycle vessels; and (d)–(f), shear rate maps of 3, 5, and 8 f–t cycle vessels.

calculated from the difference of systolic and diastolic pressures, and mean pressure (MP) from the averaged pressure within a cycle. For 3, 5, and 8 f–t cycle vessels, PP and MP were 31.9 and 98.5 mmHg, 43.4 and 100.7 mmHg, and 60.7 and 103.9 mmHg, respectively. The vessels that pertain to 3 and 8 f–t cycles had the smallest and biggest PP and MP respectively. As the vessel became stiffer, the time durations from diastolic to systolic peak pressure (0.26, 0.28, and 0.30 s) increased, and the time duration from peak systolic to dicrotic notch (0.21, 0.17, and 0.14 s) decreased, and the time duration from the dicrotic notch to end diastole increased.

D. Two-Dimensional Distribution of Flow Velocity and Shear Rate

The instantaneous 2-D maps of flow velocity and shear rate can be obtained. The typical flow patterns at peak systole were shown in Fig. 6 with arrows showing magnitude and direction, and color denoting contour. The maps of velocity vector in the left column showed parabolic profiles. The flow velocity maximized at the centerline, and gradually decreased to zero at the boundaries. The maps of shear rate in the right column demonstrated that this property is maximized near the walls.

The time-dependent waveforms of the peak velocities measured by EchoPIV were depicted in Fig. 7(a). Measurements starting from soft to stiff vessels result in the peak systolic and end diastolic velocities with magnitudes of 55.0 and 12.3 cm/s, 50.0 and 13.4 cm/s, and 44.9 and 14.8 cm/s. To evaluate the accuracy of EchoPIV measurements, the peak velocity deduced from radial velocity profiles in the vessel were compared with the profile obtained from Doppler velocity spectrum. The results were shown in Fig. 7(b)–(d). The Doppler-measured peak systolic velocities were 57.0, 53.3, and 47.2 cm/s, slightly bigger than the EchoPIV-measure values. The biases were below 5% during the whole cardiac cycle. Fig. 7(e) shows the near-wall

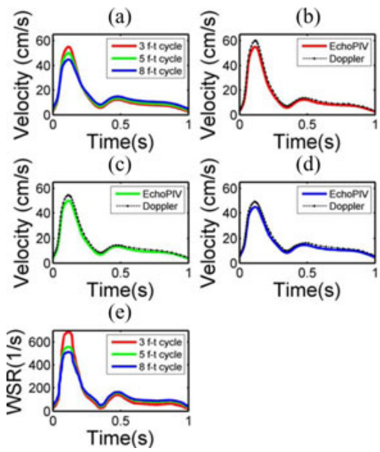

Fig. 7. Time-dependent waveforms of the peak velocities and shear rates: (a) the waveforms of peak velocities measured by EchoPIV; (b)–(d) the comparison between the waveforms of EchoPIV-measured peak velocities and the ultrasonic Doppler spectrum: (b) 3-ft-cycle vessel; (c) 5-ft-cycle vessel; (d) 8-ft-cycle vessel; and (e) the time-dependent waveform of wall shear rate close to the near wall.

shear rate plotted against time for different vessels. The maximum shear rates were 650, 550, and 500 (1/s), respectively.

IV. Discussion

In this study, three elastic vessel phantoms with identical structure and different stiffness were made from PVA-C and used in the same fluid circuit. Under the pulsatile flow condition, the vessels underwent cyclic dilation and contraction during one cardiac cycle. The recorded vessel wall distension waveform (see Fig. 4) of the vessel is similar to that of an asymptomatic common carotid artery [39]. While it is easy to understand that a stiffer vessel would undergo smaller wall motions, it is also interesting to observe that it took longer time to achieve maximum inner diameter for a stiffer vessel. The increased vessel stiffness had degraded deformation ability in response to an applied force.

The flow pressure waveforms (see Fig. 5) revealed significant information on the systolic and diastolic pressure, PP, and MP. For instance, the 8 f–t vessel pertains to the largest PP and MP. This confirmed the correlation between hypertension and artery stiffening. The time to achieve peak systolic pressure in the pressure waveform coincided with the time to achieve maximum inner diameter in the wall distension waveform. This indicates that the wall motion and flow pressure was synchronous. Another point to note is that the stiffer vessel reached the dicrotic notch earlier. The reason could be the earlier arrival of the reflection wave for the stiffer vessel.

The EchoPIV technique enabled the measurements of 2-D color flow velocity vector maps, and thus the calculation of detailed shear rate values at different locations in the flow. From the typical 2-D maps of velocity at the peak systole, we examined the parabolic flow velocity profiles for all the vessels (see Fig. 6). The shear rate maximized at the boundaries and minimized in the center. The comparison of time-dependent EchoPIV-measured peak velocities with the profile of Doppler velocity spectrum validated the measuring accuracy (see Fig. 7). In one cardiac cycle, the cyclic change of the near-wall shear rate was synchronous with that of the flow velocity. For the vessel phantoms of a regular shape, the stiffer one resulted in smaller peak velocity in the lumen center and shear rate close to the walls at the peak systole.

Considering that the endothelium is very sensitive to shear stress, local hemodynamic conditions such as low and oscillating shear can result in abnormal and disarrayed endothelial cells and increase in the intercellular permeability and the vulnerability of these vessel segments to atherosclerosis, and consequently lead to various cardiovascular events. This indicates that the reduced WSS due to increased vessel stiffness can initiate the atherosclerotic process. Further hemodynamic and pathological studies can be performed in animal models.

The usage of deionized water as the working fluid in the Harvard blood pump may cause some drawbacks in the experimental setup. Water has smaller viscosity and density as compared to real human blood, which may affect the flow velocity distribution and influence the WSS. Synthetic blood based on realistic viscosity is desirable in the future work. The pump cannot ideally simulate the real function of a human heart, and the impact of wave reflections at tube connections would inevitably influence the pressure waveforms and the velocity waveforms. Nonetheless, since we only substituted the vessel phantoms and remained other components the same throughout all the experiments, the comparison between the results of different vessel phantoms can cancel out the resulting errors. The measured results of this study demonstrated that the experimental configuration did simulate the blood flow in the artery very well, and the use of elastic vessel phantoms of different stiffness indeed provided a way to study the impact of arterial stiffness on flow dynamics. Also, EchoPIV was proven to be a useful and powerful tool in blood flow dynamics studies.

V. Conclusion

We have fabricated elastic vessel phantoms of different stiffness with PVA-C and successfully generated pulsatile flows in the vessels using a circulatory rig. Using the EchoPIV to provide accurate measurements of 2-D instantaneous and time-dependent flow velocity and shear rate vector fields in the vessel allow us to study three different vessels and demonstrate that the vessel stiffness can influence vessel wall distension, flow pressure, and time-dependent flow velocity and WSS. A decrease in wall shear rate was observed for a stiffer vessel, and this factor may function to prompt the pathological development of the endothelial cells. In future, more sophisticated-shaped phantoms (such as bifurcation or stenosis) and preclinical and clinical studies may be studied using the framework proposed in this paper.

References

[1] C. S. Roy, "The elastic properties of the arterial wall," *J. Physiol.*, vol. 3, pp. 125–159, 1881.

[2] T. Young, "Hydraulic investigations, subservient to an intended Croonian lecture on the motion of the blood," *Philosoph. Trans. Roy. Soc. London*, vol. 98, pp. 164–186, 1808.

[3] R. Botnar, G. Rappitsch, M. Beat Scheidegger, D. Liepsch, K. Perktold, and P. Boesiger, "Hemodynamics in the carotid artery bifurcation: A comparison between numerical simulations and in vitro MRI measurements," *J. Biomech.*, vol. 33, pp. 137–144, 2000.

[4] D. Liepsch, "Biofluid mechanics-an interdisciplinary research area of the future," *Technol. Health Care*, vol. 14, pp. 209–214, 2006.

[5] O. Greil, T. Kleinschmidt, W. Weiss, O. Wolf, P. Heider, S. Schaffner, M. Gianotti, T. Schmid, D. Liepsch, and H. Berger, "Flow velocities after carotid artery stenting: Impact of stent design. A fluid dynamics study in a carotid artery model with laser Doppler anemometry," *Cardiovasc. Intervent. Radiol.*, vol. 28, pp. 66–76, 2005.

[6] J. Mejia, B. Ruzzeh, R. Mongrain, R. Leask, and O. F. Bertrand, "Evaluation of the effect of stent strut profile on shear stress distribution using statistical moments," *Biomed. Eng. Online*, vol. 8, pp. 1–10, 2009.

[7] G. Choi, C. P. Cheng, N. M. Wilson, and C. A. Taylor, "Methods for quantifying three-dimensional deformation of arteries due to pulsatile and nonpulsatile forces: Implications for the design of stents and stent grafts," *Ann. Biomed. Eng.*, vol. 37, pp. 14–33, 2009.

[8] R. Aaslid, T.-M. Markwalder, and H. Nornes, "Noninvasive transcranial Doppler ultrasound recording of flow velocity in basal cerebral arteries," *J. Neurosurg.*, vol. 57, pp. 769–774, 1982.

[9] J. R. Overbeck, K. W. Beach, and D. E. Strandness, "Vector Doppler: Accurate measurement of blood velocity in two dimensions," *Ultrasound Med. Biol.*, vol. 18, pp. 19–31, 1992.

[10] L. Sandrin, S. Manneville, and M. Fink, "Ultrafast two-dimensional ultrasonic speckle velocimetry: A tool in flow imaging," *Appl. Phys. Lett.*, vol. 78, pp. 1155–1157, 2001.

[11] J. Udesen, F. Gran, K. Hansen, J. A. Jensen, C. Thomsen, and M. B. Nielsen, "High frame-rate blood vector velocity imaging using plane waves: Simulations and preliminary experiments," *IEEE Trans. Ultrason., Ferroelectr. Freq. Control*, vol. 55, no. 8, pp. 1729–1743, Aug. 2008.

[12] B. Beulen, A. C. Verkaik, N. Bijnens, M. Rutten, and F. van de Vosse, "Perpendicular ultrasound velocity measurement by 2D cross correlation of RF data. Part B: Volume flow estimation in curved vessels," *Experiments Fluids*, vol. 49, pp. 1219–1229, 2010.

[13] F. Zhang, C. Lanning, L. Mazzaro, A. J. Barker, P. E. Gates, W. D. Strain, J. Fulford, O. E. Gosling, A. C. Shore, and N. G. Bellenger, "*In vitro* and preliminary in vivo validation of echo particle image velocimetry in carotid vascular imaging," *Ultrasound Med. Biol.*, vol. 37, pp. 450–464, 2011.

[14] H. Zheng, L. Liu, L. Williams, J. R. Hertzberg, C. Lanning, and R. Shandas, "Real time multicomponent echo particle image velocimetry technique for opaque flow imaging," *Appl. Phys. Lett.*, vol. 88, art. no. 261915, 2006.

[15] J. D. Humphrey, "Mechanisms of arterial remodeling in hypertension coupled roles of wall shear and intramural stress," *Hypertension*, vol. 52, pp. 195–200, 2008.

[16] Y. Qiu and J. M. Tarbell, "Interaction between wall shear stress and circumferential strain affects endothelial cell biochemical production," *J. Vasc. Res.*, vol. 37, pp. 147–157, 2000.

[17] Y.-S. J. Li, J. H. Haga, and S. Chien, "Molecular basis of the effects of shear stress on vascular endothelial cells," *J. Biomech.*, vol. 38, pp. 1949–1971, 2005.

[18] M.-L. M. Grønholdt, "Ultrasound and lipoproteins as predictors of lipid-rich, rupture-prone plaques in the carotid artery," *Arterioscle., Thromb., Vasc. Biol.*, vol. 19, pp. 2–13, 1999.

[19] R. H. Selzer, W. J. Mack, P. L. Lee, H. Kwong-Fu, and H. N. Hodis, "Improved common carotid elasticity and intima-media thickness measurements from computer analysis of sequential ultrasound frames," *Atherosclerosis*, vol. 154, pp. 185–193, 2001.

[20] F. U. Mattace-Raso, T. J. van der Cammen, A. Hofman, N. M. van Popele, M. L. Bos, M. A. Schalekamp, R. Asmar, R. S. Reneman, A. P. Hoeks, and M. M. Breteler, "Arterial stiffness and risk of coronary heart disease and stroke the rotterdam study," *Circulation*, vol. 113, pp. 657–663, 2006.

[21] G. F. Mitchell, S.-J. Hwang, R. S. Vasan, M. G. Larson, M. J. Pencina, N. M. Hamburg, J. A. Vita, D. Levy, and E. J. Benjamin, "Arterial stiffness and cardiovascular events the framingham heart study," *Circulation*, vol. 121, pp. 505–511, 2010.

[22] C. Vlachopoulos, K. Aznaouridis, M. F. O'Rourke, M. E. Safar, K. Baou, and C. Stefanadis, "Prediction of cardiovascular events and all-cause mortality with central haemodynamics: A systematic review and meta-analysis," *Eur. Heart J.*, vol. 31, pp. 1865–1871, 2010.

[23] K. Sutton-Tyrrell, S. S. Najjar, R. M. Boudreau, L. Venkitachalam, V. Kupelian, E. M. Simonsick, R. Havlik, E. G. Lakatta, H. Spurgeon, and S. Kritchevsky, "Elevated aortic pulse wave velocity, a marker of arterial stiffness, predicts cardiovascular events in well-functioning older adults," *Circulation*, vol. 111, pp. 3384–3390, 2005.

[24] T. W. Hansen, J. A. Staessen, C. Torp-Pedersen, S. Rasmussen, L. Thijs, H. Ibsen, and J. Jeppesen, "Prognostic value of aortic pulse wave velocity as index of arterial stiffness in the general population," *Circulation*, vol. 113, pp. 664–670, 2006.

[25] J. Luo, R. X. Li, and E. E. Konofagou, "Pulse wave imaging of the human carotid artery: An *in vivo* feasibility study," *IEEE Trans. Ultrason., Ferroelectr. Freq. Control*, vol. 59, no. 1, pp. 174–181, Jan. 2012.

[26] J. Luo and E. E. Konofagou, "Imaging of wall motion coupled with blood flow velocity in the heart and vessels *in vivo:* A feasibility study," *Ultrasound Med. Biol.*, vol. 37, pp. 980–995, 2011.

[27] S. Golemati, A. Sassano, M. J. Lever, A. A. Bharath, S. Dhanjil, and A. N. Nicolaides, "Carotid artery wall motion estimated from B-mode ultrasound using region tracking and block matching," *Ultrasound Med. Biol.*, vol. 29, pp. 387–399, 2003.

[28] T. Zakaria, Z. Qin, and R. L. Maurice, "Optical-flow-based b-mode elastography: Application in the hypertensive rat carotid," *IEEE Trans. Med. Imag.*, vol. 29, no. 2, pp. 570–578, Feb. 2010.

[29] H. Kanai, H. Hasegawa, M. Ichiki, F. Tezuka, and Y. Koiwa, "Elasticity imaging of atheroma with transcutaneous ultrasound preliminary study," *Circulation*, vol. 107, pp. 3018–3021, 2003.

[30] L. Niu, M. Qian, R. Song, L. Meng, X. Liu, and H. Zheng, "A texture matching method considering geometric transformations in noninvasive ultrasonic measurement of arterial elasticity," *Ultrasound Med. Biol.*, vol. 38, pp. 524–533, 2012.

[31] L. Niu, M. Qian, R. Song, L. Meng, X. Liu, and H. Zheng, "A 2D noninvasive ultrasonic method for simultaneous measurement of arterial strain and flow pattern," *Clin. Physiol. Funct. Imag.*, vol. 32, pp. 323–329, 2012.

[32] M. Qian, L. Niu, Y. Wang, B. Jiang, Q. Jin, C. Jiang, and H. Zheng, "Measurement of flow velocity fields in small vessel-mimic phantoms and vessels of small animals using micro ultrasonic particle image velocimetry (micro-EPIV)," *Phys. Med. Biol.*, vol. 55, pp. 6069–6088, 2010.

[33] L. Niu, M. Qian, K. Wan, W. Yu, Q. Jin, T. Ling, S. Gao, and H. Zheng, "Ultrasonic particle image velocimetry for improved flow gradient imaging: Algorithms, methodology and validation," *Phys. Med. Biol.*, vol. 55, pp. 2103–2120, 2010.

[34] K. C. Chu and B. K. Rutt, "Polyvinyl alcohol cryogel: An ideal phantom material for MR studies of arterial flow and elasticity," *Magn. Resonance Med.*, vol. 37, pp. 314–319, 1997.

[35] F. Dunn, *Ultrasonic Tissue Characterization*. New York, NY, USA: Springer-Verlag, 1996.

[36] R. Song, M. Qian, L. Niu, Q. Jin, and H. Zheng, "Multi-component hemodynamic measurement in flexible vascular phantom using echo particle image velocimetry," in *Proc. 4th Int. Conf. Biomed. Eng. Informat.*, 2011, pp. 404–407.

[37] B. Jiang, M. Qian, L. Niu, R. Song, H. Zhu, Q. Jin, and H. Zheng, "Region growing based on window frame difference for segmenting ultrasonic contrast images of arteries," in *Proc. 5th Int. Conf. Bioinformatics Biomed. Eng.*, 2011, pp. 1–4.

[38] J. Greenleaf, F. Duck, W. Samayoa, and S. Johnson, "Ultrasonic data acquisition and processing system for atherosclerotic tissue characterization," in *Proc. Ultrason. Symp.*, 1974, pp. 738–743.

[39] J. Dineley, S. Meagher, T. Poepping, W. McDicken, and P. Hoskins, "Design and characterisation of a wall motion phantom," *Ultrasound Med. Biol.*, vol. 32, pp. 1349–1357, 2006.

Ming Qian (M'12) received the B.S. degree in physics and the Ph.D. degree in optics from Nanjing University of Science and Technology, China, in 2003 and 2008, respectively.

He joined Shenzhen Institutes of Advanced Technology, Chinese Academy of Sciences in 2008 as an Assistant Professor, and was then promoted to be Associate Professor in 2011. His research interests include ultrasonics, ultrasonic imaging, ultrasonic transducer design and fabrication, and also signal and image processing. He has published more

than 40 peer-reviewed journal papers and international conference proceedings with more than 30 indexed by SCI/EI, and applied more than 10 patents. He is principal investigator of more than ten projects including National Key Technology R&D Program of China, National Natural Science Foundation Grant of China, etc.

Dr. Qian is a member of the EMBC, committee member of the acoustical society of China, and the referees for funding agencies National Natural Science Foundation of China and Natural Science Foundation of Guangdong Province. He is the reviewer of Ultrasound in Medicine and Biology, Ultrasonics, PLOS One, IEEE TRANSACTIONS ON BIOMEDICAL ENGINEERING, *Journal of Biomechanics*, etc.

Lili Niu received the Master's degree in biomedical engineering from Northeast University, China, in 2009, and the Ph.D. degree in computer application technology from the Chinese Academy of Sciences (CAS), in 2012.

She is now an Assistant Professor at the Shenzhen Institute of Advanced Technology, CAS. Her main research interests include developing advanced biomedical ultrasound techniques for measuring vascular biomechanics, ultrasound contrast imaging, and high-frequency ultrasound imaging. She has published more than ten peer-review journals in the biomedical engineering field.

Kelvin Kian Loong Wong was born in Singapore in 1976. He received the B.Eng. (Hons.) degree in mechanical and production engineering from Nanyang Technological University, Singapore, in 2001, the MAIT degree in applied information technology from The University of Sydney, Australia, in 2003, and the Ph.D. degree in electrical and electronic engineering from The University of Adelaide, Australia, in 2009, mainly under the supervision of Jagannath Mazumdar and Derek Abbott.

He has more than 5 years of medical imaging and computational modeling and simulation experience. From 2006 to 2009, he was doing research work on medical imaging and cardiac flow analysis. Since 2009 to now, he was involved in computational fluid and solid dynamics. In 2013, he began working on discrete element method with applications in biological systems. He is the author of the book "*Methods in Research and Development of Biomedical Devices*," and has served as Associate Editors for journals in the area of biomedical engineering. He is currently an Assistant Professor in the School of Computer Science and Software Engineering at The University of Western Australia. His publications now span a diverse range of research fields, including physics, applied mathematics, mechanics, cardiac flow analysis, multiscale modeling, medical imaging, medical image reconstruction, discrete element method, computational fluid dynamics, and biomedical device production.

Derek Abbott (M'85–SM'99–F'05) was born in South Kensington, London, U.K., in 1960. He received the B.Sc. (Hons.) degree in physics from Loughborough University, Leicestershire, U.K., in 1982 and the Ph.D. degree in electrical and electronic engineering from The University of Adelaide, S.A. Australia, in 1995, under K. Eshraghian and B. R. Davis.

From 1978 to 1986, he was a Research Engineer at the GEC Hirst Research Centre, London, U.K. From 1986 to 1987, he was a VLSI Design Engineer at Austek Microsystems, Australia. Since 1987, he has been with The University of Adelaide, where he is presently a Full Professor with the School of Electrical and Electronic Engineering. He coedited *Quantum Aspects of Life* (London, U.K.: Imperial College Press, 2008), coauthored *Stochastic Resonance* (Cambridge, U.K.: Cambridge University Press, 2008), and coauthored *Terahertz Imaging for Biomedical Applications* (New York, NY, USA: Springer-Verlag, 2012). He holds more than 800 publications/patents and has been an invited speaker at more than 100 institutions. His research interests include the area of multidisciplinary physics and electronic engineering applied to complex systems. His research programs span a number of areas of stochastics, game theory, photonics, biomedical engineering, and computational neuroscience.

Prof. Abbott is a Fellow of the Institute of Physics. He has won a number of awards including the South Australian Tall Poppy Award for Science (2004), the Premier's SA Great Award in Science and Technology for outstanding contributions to South Australia (2004), and an Australian Research Council Future Fellowship (2012). He has served as an Editor and/or Guest Editor for a number of journals including the *IEEE Journal of Solid-State Circuits*, *Journal of Optics B*, the *Microelectronics Journal, Chaos, Smart Structures and Materials*, *Fluctuation Noise Letters, PLOSONE*, and is currently on the editorial boards of the *Proceedings of the IEEE*, and the *IEEE Photonics Journal*.

Qifa Zhou (SM'11) received the Ph.D. degree from the Department of Electronic Materials and Engineering at Xi'an Jiaotong University, China, in 1993.

He is currently a Research Professor at the NIH Resource on Medical Ultrasonic Transducer Technology and the Department of Biomedical Engineering and Industry and System Engineering at the University of Southern California (USC), Los Angeles, CA, USA. Before joining USC in 2002, he worked in the Department of Physics at Zhongshan University of China, the Department of Applied Physics at Hong Kong Polytechnic University, and the Materials Research Laboratory at Pennsylvania State University. His current research interests include the development of piezoelectric high-frequency ultrasound transducers for medical imaging applications such as photoacoustic imaging, intravascular imaging and cell–tissue imaging. He has published more than 150 journal papers in this area.

Dr. Zhou is a Fellow of SPIE and AIMBE, a senior member of the IEEE Ultrasonics, Ferroelectrics, and Frequency Control (UFFC) Society and a member of the Ferroelectric Committee, UFFC in IEEE. He is also a member of the technical program Committee of IUS in IEEE and Photoacoustic Committee in SPIE. He is an Associate Editor of IEEE UFFC.

Hairong Zheng (SM'11) received the B.S. degree from the Harbin Institute of Technology, China, in 2000 and the Ph.D. degree in mechanical engineering from the University of Colorado at Boulder, USA, in 2006.

He joined the University of California, Davis, USA, first as a Postdoctoral Fellow, and then as a Project Scientist in the Biomedical Engineering Department. He is now a Full Professor and the Director of the Institute of Biomedical and Health Engineering, Shenzhen Institutes of Advanced Technology, Chinese Academy of Sciences. His research areas have been focused on developing ultrasonic techniques and systems for imaging, drug delivery, and therapy, and multimodality medical imaging systems. He has published more than 100 peer-reviewed journal papers and international conference proceedings.

Dr. Zheng is a recipient of the American Heart Association Pre-Doctoral Fellowship (2005). He is a committee member of the IEEE-EMBS technique standard association, editor of Ultrasound in Medicine and Biology, committee member of Ultrasound in Medicine, the acoustical society of china, standing committee member of imaging physics and technology society, standing committee member of molecular imaging society, committee member of young association of the Chinese academy of science, the chairman of IEEE Shenzhen Chapter.